Available online at www.sciencedirect.com
ScienceDirect
Catalysis Today 119 (2007) 39–43
CATALYSIS TODAY
www.elsevier.com/locate/cattod

# Hydrodenitrogenation of indole over $Mo_2C$ catalyst: Insights into mechanistic events through DFT modeling

Witold Piskorz [a,*], Grzegorz Adamski [a], Andrzej Kotarba [a], Zbigniew Sojka [a,b], Céline Sayag [c], Gérald Djéga-Mariadassou [c]

[a] *Faculty of Chemistry, Jagiellonian University, Ingardena 3, 30-060 Cracow, Poland*
[b] *Regional Laboratory of Physicochemical Analyses and Structural Research, Ingardena 3, 30-060 Cracow, Poland*
[c] *Université P. et M. Curie, Laboratoire Réactivité de Surface, UMR CNRS 7609, 4, Place Jussieu, Case 178, 75252 Paris Cedex 05, France*

Available online 18 September 2006

**Abstract**

The molecular reaction mechanism of hydrodenitrogenation of indole was studied using density-functional theory calculations of the adsorbed *o*-ethylaniline surrounded by mobile hydrogen atoms. It was found that the hydrogenation of *o*-ethylaniline occurs through two steps: consisting in redistribution of the π electron density to form multiple partial Mo–C(ring) bonds with the surface upon adsorption, and a subsequent hydrogen attack directed on the aromatic ring or the amine group. The direction of the hydrogen attack and the associated energy barriers determine the rate constants of the early (DDN, direct denitrogenation) and late (HYD, hydrogenation) nitrogen removal steps, and thus rules the selectivity of indole hydrodenitrogenation to ethylcyclohexane or ethylbenzene.


*Keywords:* $Mo_2C$; Catalyst; HDN; Hydrodenitrogenation; Indole; DFT

## 1. Introduction

Interstitial carbides of early transition metals (TMCs) have attracted a considerable attention in last decades. Much of this interest can be attributed to their unique physical and chemical properties resulting in a spectacular catalytic behavior [1,2]. These materials often exhibit catalytic advantages over their parent metals in activity, selectivity, and resistance to poisoning. They are capable of adsorbing hydrogen, its activation and transfer to the reactant molecules. Hence, carbides exhibit high catalytic activity for reactions involving hydrogen transfer, such as hydrogenation, hydrogenolysis, isomerization, and, more recently, deep hydrodenitrogenation (HDN) and hydrodesulphurization (HDS) processes [3–5].

Among the TMCs, hexagonal $Mo_2C$ bulk and supported catalysts were found to be one of the most active in HDN process [3]. They have been found to be comparable to industrial CoMo and NiMo catalysts in nitrogen removal from N-containing model compounds representative for heavy fraction derived from petroleum, such as indole [6] or carbazol [7].

The reaction networks of hydrotreating processes are usually complex and involve number of individual steps. It appears that in most cases hydrogenation of heteroatom ring occurs prior to C–N bond breaking. Generally, the reaction proceeds in two parallel routes leading to direct (DDN) or indirect (HYD) nitrogen removal depending on the hydrogen attack on the heterocyclic or carbocyclic ring, respectively [8]. The catalytic data can be interpreted in terms of kinetic coupling of those cycles through a common intermediate, scrutinized recently at both conceptual and formal levels by Djéga-Mariadassou and Boudart [9], and widely applied in practice [10–12]. The relative rates of both pathways determine aromatics versus aliphatic compounds selectivity of the catalyst, which is of practical concern.

In this paper we use density-functional theory (DFT) calculations to get an insight into the mechanism of the heteroatom removal process in HDN of indole over $Mo_2C$ catalyst. The two possible pathways of the reaction are analyzed in terms of the hydrogen attack direction on *o*-ethylaniline, a most abundant reaction intermediate adsorbed on the catalyst surface.

* Corresponding author.
*E-mail address:* wpiskorz@chemia.uj.edu.pl (W. Piskorz).

0920-5861/$ – see front matter © 2006 Elsevier B.V. All rights reserved.
doi:10.1016/j.cattod.2006.08.050

## 2. Methods

For DFT [13–15] computations the $Mo_2C$ catalyst was modeled with the $Mo_{24}C_6$ cluster previously described elsewhere [16]. Calculations were performed with the DMol-960 [17] program (implementing Delley's scheme [18]) using local density approximation with the VWN correlation-exchange potential [19] and the DNP basis set (double numerical augmented by polarization functions). The VWN potential was chosen because of its high computational performance, yielding despite of its limitations a rather good accuracy for systems containing heavy metal atoms with large number of electrons [20–22].

The integration was performed over the standard (medium) density of the grid [23]. The geometry of cluster was fully optimized using numerical gradients and the BFGS (Broyden–Fletcher–Goldfarb–Shanno) Hessian update method [24]. The SCF electron density convergence criterion was set at $10^{-6}$ a.u. The optimization was based on the gradient displacement norms ($10^{-3}$ a.u.) and threshold for energy set at $10^{-5}$ a.u. The electronegativity, $\chi = -(\partial E/\partial n)_V$, where $E$ is the total energy, $n$ the number of electrons, and $V$ is the potential generated by the nuclei of reactants, was obtained from the finite-difference approximation of the derivative by solving the parabolic equation $E = \eta n^2 + \chi n + \text{const}$, for the energies of the corresponding anions, neutrals and cations. The population analysis was based on the Hirshfeld procedure [25,26], and the bond orders were calculated within the Mayer scheme [27,28].

For mapping the potential energy surface of hydrogen migration on the $Mo_2C$ cluster the $x$, $y$-coordinates of H atom were paced with a step of 0.1 nm within the rectangle of 0.6 nm × 0.9 nm, and the $z$ distance was optimized at each point of the grid formed.

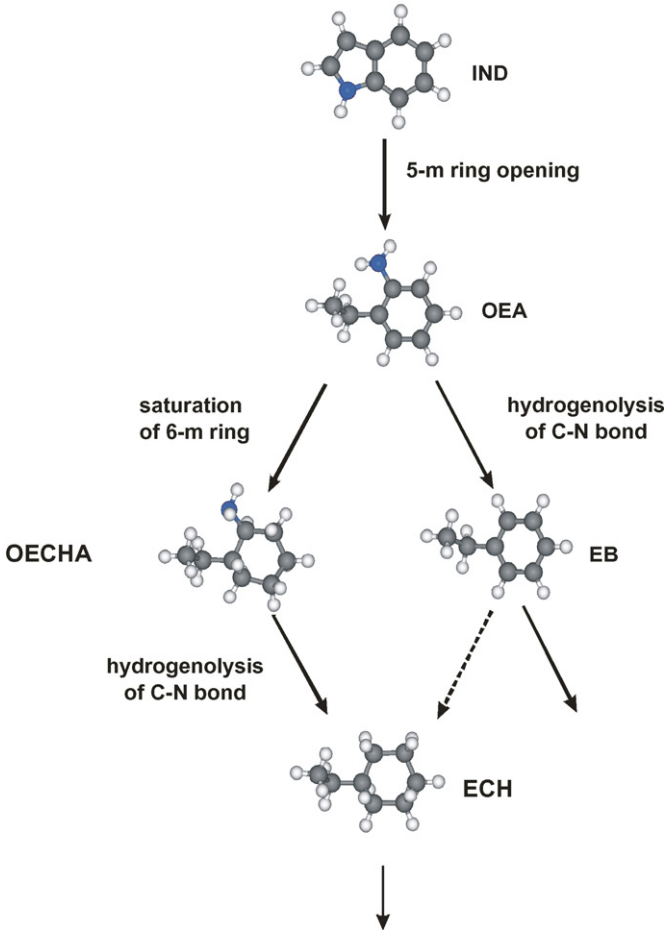


Fig. 1. Schematic network of consecutive-parallel reactions used for kinetic modeling of HDN of indole.

## 3. Results and discussion

### 3.1. Reaction network

The isothermal kinetic studies of indole HDN were carried out over $Mo_2C$ catalysts and the results were discussed in our previous paper [8]. As shown in the scheme (Fig. 1) the loop network of consecutive-parallel reactions involves *o*-ethylaniline (OEA) as common intermediate and two final products (ethylbenzene (EB) and ethylcyclohexane (ECH)). The HDN reaction of indole, after its initial hydrogenation to indoline and C–N bond hydrogenolysis to OEA, splits into two routes. The first one (DDN) starts from OEA leading through dihydroaniline intermediate to EB as a terminal product. The second one (HYD) proceeds via hydrogenation of OEA to *o*-ethylcyclohexylamine (OECHA), and finally to ECH. These two pathways are additionally coupled by the transformation of EB to ECH [11,12]. Further information concerning the detailed kinetics rationalizing the global model can be found elsewhere [8].

### 3.2. Adsorption of reactants

While considering a catalytic system the strength of mutual interactions at first approach can be judged from the global reactivity descriptors: chemical potential and hardness of the reactants [29]. In the case of the HDN process of OEA on $Mo_2C$, taking into account that the chemical potential of the catalyst $\mu_{Mo_2C} = E_F = -3.53$ eV [16] and $\mu_{OEA} = -3.55$ eV, we may expect, owing to the close matching of the surface and adsorbate chemical potentials, a strong mutual electronic interaction of OEA with the $Mo_2C$ surface.

The DFT calculations revealed that the dissociative adsorption of hydrogen molecule on $Mo_2C$ is a non-activated process. The resultant atomic radicals are negatively charged with $q_H$ varying from −0.11 to −0.13. Since the availability of active hydrogen on catalyst surface is the essential requirement for any hydroprocessing reaction to occur, the mobility of the surface $H^{\delta-}$ atoms was investigated by mapping the potential energy with respect to their position on the cluster (*vide infra*). The results revealed that hydrogen atoms are quite mobile at the reaction temperature. The highest binding energy of the hydrogen atom was observed for the hollow position between two adjacent Mo atoms, whereas, the lowest one was found above the molybdenum with the octahedral holes occupied by the interstitial carbons. The local maxima correspond to atomic hydrogen adsorbed on Mo atop positions above empty octahedral holes. The resulting low energy diffusion channel has a barrier of 0.27 eV passing

across hollow and atop position distal from interstitial carbon. The other channels exhibit higher activation barrier for hydrogen diffusion varying from 0.51 to 1.2 eV. The obtained barriers are in line with the experimentally determined value of activation energies (<0.9 eV) determined for $H_2/D_2$ isotopic exchange over these catalysts constrained by the surface diffusion of reactants [30].

Since hydrogen molecules readily dissociate homolytically and the resultant H atoms are quite mobile, the rates of the DDN and HYD routes are essentially controlled by the activation of OEA, the direction of the hydrogen attack, and the barrier of its insertion into this common intermediate.

The structure of the OEA molecule adsorbed on the $Mo_2C$ surface is shown in Fig. 2. The selected geometrical parameters, Hirshfeld charges and Mayer bond orders for the OEA in the gas phase and after adsorption are collected in Table 1. Adsorption of OEA on the surface of $Mo_2C$ results in strong geometric distortion and redistribution of the electronic density. The greatest changes were observed in the aromatic ring, which undergoes a pronounced dearomatization. This can be readily inferred from the increase in the C–C(ring) bond lengths from 1.39–1.40 to 1.43–1.48 Å, and the associated decrease in the bond orders from 1.262–1.392 to 0.994–1.106. The deformation of the aromatic ring toward a twisted boat-like structure is reflected by the departure from the ring planarity gauged by dihedral angles $\theta = -21.9^\circ$ and $+19.8^\circ$. The negative charges on carbon atoms strongly increased, with the greatest changes observed at the carbons connected with the both functional groups, whereas the positive charges on the hydrogen atoms remained approximately the same. The Mo–C(ring) distance 2.03–2.47 Å and the bond orders 0.284–0.612 indicate that new quite strong partial bonds between the carbon ring and the surface molybdenum atoms are formed at the expense of the π electron density. Neglecting the appreciable deviation in the orientation of the ethyl group with respect to the aromatic ring, the geometry of the ethyl remains practically intact. In contrast, for the amine group the C–N bond is stretched from 1.39 to 1.45 Å, which is accompanied by the decrease in the bond order from 1.172 to 1.018. However, the most significant change here consisted in the reversal of the partial charge on the $C_2$ carbon from +0.0327 to −0.0106. The resultant profound structural and charge modifications lead to the significant enhancement of the electric dipole moment of the adsorbed OEA from 1.73 to 3.30 D.

Table 1
Principal changes in geometric parameters, Mayer bond orders and Hirshfeld partial charges within the OEA molecule upon adsorption on the $Mo_{24}C_6$ cluster

| Atoms | OEA gas phase | OEA adsorbed on $Mo_2C$ |
|---|---|---|
| Bond lengths (Å) | | |
| C–C(ring) | 1.39–1.40 | 1.43–1.48 |
| $C_2$–$C_3$(ring) | 1.40 | 1.47 |
| C–N | 1.39 | 1.45 |
| Mo–C(ring) | – | 2.03–2.43 |
| Mo–C(ethyl) | – | 3.42 |
| Mo–N | – | 2.41 |
| Angles (°) | | |
| C–C–C(ring) | 118.5–122.0 | 115.6–122.0 |
| $C_1$–$C_2$–$C_3$(ring) | 118.5 | 122.0 |
| Dihedral angle | | |
| $C_3$–$C_4$–$C_5$–$C_6$ | 1.6 | −21.9 |
| $C_3$–$C_2$–$C_1$–$C_6$ | −1.6 | 19.8 |
| Mayer bond order | | |
| C–C(ring) | 1.262–1.392 | 0.994–1.106 |
| $C_2$–$C_3$(ring) | 1.262 | 0.994 |
| C–N | 1.172 | 1.018 |
| N–H | 0.727, 0.861 | 0.644, 0.765 |
| Mo–C(ring) | – | 0.284–0.612 |
| Mo–N | – | 0.345 |
| Hirshfeld charges | | |
| $C_1$, $C_2$ | −0.0769, 0.0327 | −0.1313, −0.0106 |
| $C_3$, $C_4$ | −0.0168, −0.0595 | −0.0603, −0.0973 |
| $C_5$, $C_6$ | −0.0754, −0.0618 | −0.1205, −0.0833 |
| N | −0.1778 | −0.1421 |

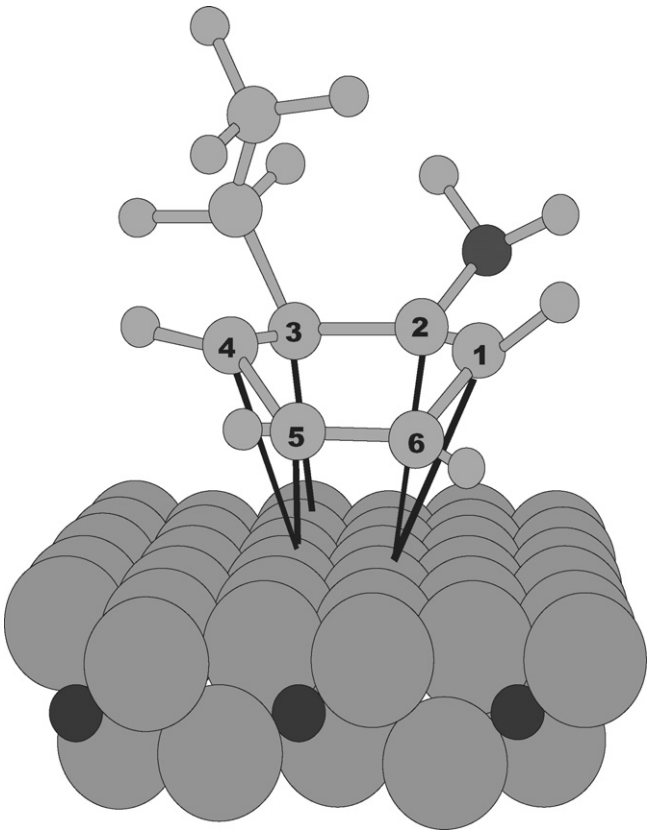

Fig. 2. Optimized structures of the OEA molecule adsorbed on $Mo_{24}C_6$ cluster.

It is clear that the adsorbed OEA forms strong multiple partial bonds with the surface, mainly at the expense of the OEA ring and also, to a lesser extent, of the cluster Mo–Mo and Mo–C bonds. Indeed, the surface–OEA complex involves six Mo atoms with the total bond order of 3.359. The sum of bond orders in the aromatic ring in OEA molecule decreased from 8.048 to 6.301 upon adsorption.

In conclusion, the formation of OEA–$Mo_2C$ surface complex, with strongly chemisorbed and deeply dearomatized *o*-ethylaniline moiety, creates a new reactive intermediate that actually is the target of the hydrogen attack.

### 3.3. Reaction mechanism

Combining the catalytic data with the results of DFT calculations of hydrogen and OEA adsorption allowed for the development of a model of reactive ensemble on the $Mo_2C$ surface. The active ensemble of the indole HDN reaction on the $Mo_2C$ surface is constituted by an adsorbed OEA and a profusion of mobile hydrogen atoms. The OEA enters into the DDN or HYD cycles, depending on the direction of the attack of the mobile surface H atoms on the adsorbed molecule. The progress of the reaction can be followed by analyzing the evolution of the appropriate bond orders: N–H and N–C(ring) for DDN, or C(ring)–Mo and C(ring)–H for HYD, as the hydrogen adatom approaches the OEA intermediate (Fig. 3a and b, respectively). In the first pathway (H atom attack on the $NH_2$ group) the N–C(ring) bond order decreases by about 0.2, whereas, the N–H bond is formed (bond order changes from 0 to 0.8). For the latter pathway (H atom attack onto the aromatic ring), a monotonous decrease in the C–Mo bond order by 0.4 is accompanied by an increase in the carbon–hydrogen bond order by 0.8. These results indicate that the new C–H bond is formed at the expanse of the anterior bond between the OEA molecule and the surface molybdenum. Thus, the hydrogenation of *o*-ethylaniline can be regarded as a two step process: initial redistribution of the π electron density to form multiple partial

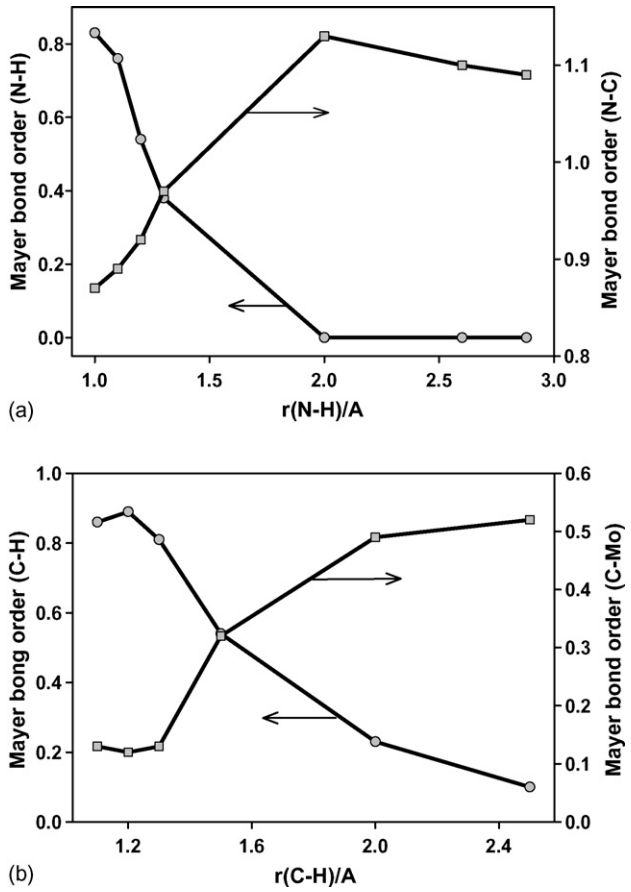


Fig. 3. Changes in the Mayer bond orders of N–H and N–C(ring) and C(ring)–H and C(ring)–Mo as a function of the distance upon hydrogen attack on amine group (a) or aromatic cycle (b) of the adsorbed OEA intermediate.

Mo–C bonds with the surface and their subsequent erosion by the hydrogen attack, giving rise to the C–H bond formation. The rates of the DDN and HYD pathways are then molecularly controlled by the specific electronic structure of the surface complex (chemisorbed OEA surrounded by itinerant H atoms) and by the energetic barriers of the apposite hydrogen insertion locus. The difference in the calculated activation energies of the DDN and HYD pathways was found to be 8 kcal $mol^{-1}$ in favor of the HYD process. This accounts for experimentally observed preferential ring hydrogenation route ($k_{HYD} = 18 \pm 1\ s^{-1}$) over the direct dehydrogenation ($k_{DDN} = 12 \pm 1\ s^{-1}$). Thus, the results of quantum-chemical modeling explain at the molecular level the selectivity ratio for aromatic (DDN) and aliphatic (HYD) products observed in our previous work [8].

## 4. Conclusions

Insight into the molecular reaction mechanism of indole hydrodenitrogenation over $Mo_2C$ was provided by DFT calculations. Formation of a strong OEA–$Mo_2C$ surface–π complex, with deeply dearomatized *o*-ethylaniline moiety was shown. The direction of the H attack on the ring or amine group of the OEA intermediate was proposed to account for the reaction selectivity. The calculated difference in energy barriers (8 kcal $mol^{-1}$) between the DDN and HYD routes provides a molecular rationale for the observed higher rates of aromatics (EB) versus aliphatic (ECH) production.

## Acknowledgements

This work was done within Research Project no. 3T09A17219, sponsored by the Polish State Committee for Scientific Research (KBN) and French-Polish cooperation program JUMELAGE ‘‘Carbonaceous and Catalytic Materials for Environment’’ financed by CNRS and KBN.

## References

[1] S.T. Oyama, The Chemistry of Transition Metal Carbides and Nitrides, Blackie Academic & Professional, Glasgow, 1996.
[2] L.I. Johansson, Surf. Sci. Rep. 21 (1995) 177.
[3] E. Furimsky, App. Catal A: Gen. 240 (2003) 1.
[4] J.C. Schlatter, S.T. Oyama, J.E. Metcalf, J.M. Lambert, Ind. Eng. Chem. Res. 27 (1988) 1648.
[5] S. Ramanathan, S.T. Oyama, J. Phys. Chem. 99 (1995) 16365.
[6] S. Li, J.S. Lee, T. Hyeon, K.S. Suslick, Appl. Catal. A: Gen. 184 (1999) 1.
[7] A. Szamańska, M. Lewandowski, C. Sayag, G. Djega-Mariadassou, J. Catal. 218 (2003) 24.
[8] G. Adamski, K. Dyrek, A. Kotarba, Z. Sojka, C. Sayag, G. Djéga-Mariadassou, Catal. Today 90 (2004) 115–119.
[9] G. Djéga-Mariadassou, M. Boudart, J. Catal. 216 (2003) 89.
[10] M.J. Girgis, B.C. Gates, Ind. Eng. Chem. Res. 30 (1991) 2021.
[11] K. Miga, K. Stańczyk, C. Sayag, D. Brodzki, G. Djéga-Mariadassou, J. Catal. 183 (1999) 63.
[12] H. Abe, A.T. Bell, Catal. Lett. 18 (1993) 1.
[13] P. Honenberg, W. Kohn, Phys. Rev. 136 (1964) 864.
[14] W. Kohn, L.J. Sham, Phys. Rev. 140 (1965) 1133.
[15] R.G. Parr, W. Yang, Density-Functional Theory of Atoms and Molecules, Oxford University Press, Oxford, 1989.

[16] A. Kotarba, G. Adamski, W. Piskorz, Z. Sojka, C. Sayag, G. Djega-Mariadassou, J. Phys. Chem. B 108 (2004) 2885.
[17] D. Mol, InsightII, Release 960, Biosym/MSI, San Diego, 1995.
[18] B. Delley, J. Chem. Phys. 92 (1990) 508.
[19] S.H. Vosko, L. Wilk, M. Nusair, Can. J. Phys. 59 (1990) 1200.
[20] E. Broclawik, A. Góra, P. Liguzinski, P. Petelenz, M. Slawik, Catal. Today 101 (2) (2005) 155.
[21] P. Kornelak, A. Michalak, M. Najbar, Catal. Today 101 (2) (2005) 175.
[22] A.S. Shalabi, Appl. Surf. Sci. 221 (2004) 53.
[23] A. Goursot, I. Pàpai, C.A. Daul, Int. J. Quant. Chem. 52 (1994) 799.
[24] H.B. Schlegel, in: K.P. Lawley (Ed.), Ab initio Methods in Quantum Chemistry I, Wiley, New York, 1987.
[25] F.L. Hirshfeld, Theor. Chim. Acta B 44 (1977) 129.
[26] E.R. Davidson, S. Chakravorty, Theor. Chim. Acta 83 (1992) 319.
[27] I. Mayer, Chem. Phys. Lett. 97 (1983) 270.
[28] I. Mayer, Chem. Phys. Lett. 110 (1984) 440.
[29] R.G. Pearson, Chemical Hardness, Wiley–VCH, Weinheim, 1997.
[30] G. Adamski, PhD Thesis, Jagiellonian University, 2004.